International Forum on Aeroelasticity and Structural Dynamics
IFASD 2017
25-28 June 2017, Como - Italy

EXPERIMENTAL INVESTIGATION OF FLUTTER BOUNDARY WITH CONTROLLED VIBRATION LEVELS

Jurij Sodja[1], Federico Roizner[2], Roeland De Breuker[1], and Moti Karpel[2]

[1] Faculty of Aerospace Engineering
Delft University of Technology
j.sodja@tudelft.nl, r.debreuker@tudelft.nl

[2] Faculty of Aerospace Engineering
Technion - Israel Institute of Technology
froizner@campus.technion.ac.il, karpel@technion.ac.il

Keywords: experimental aeroelasticity, parametric flutter margin, flutter, divergence.

Abstract: The first experimental application of the Parametric Flutter Margin method for identification of aeroelastic instabilities is presented. The experiment was performed in two steps using a two degree-of-freedom wing model mounted in the wind tunnel. First, the reference flutter and divergence conditions were found by increasing the airstream velocity until the observed response diverged. Then, the system was stabilized according to the Parametric Flutter Margin methodology, and the flutter and divergence conditions of the original wing were identified positively while being in a stable regime demonstrating excellent agreement with the reference instability conditions. Although, the new experimental methodology is not model based, the results were compared with a theoretical model showing good agreement as well. The acquired data proves both the accuracy of the Parametric Flutter Margin method as well as its capability to test for aeroelastic instabilities, both flutter and divergence, in stable and predictive testing conditions.

1 INTRODUCTION

Flight testing, used to prove that the aircraft flight envelope is flutter free is a dangerous and laborious task. The flutter boundary is cautiously approached by gradually increasing the flight speed until the flight envelope is reached or a damping coefficient reaches the 3% threshold. Meanwhile the aircraft response to various sources of excitation like atmospheric turbulence and control surface deflections is constantly being monitored and analysed. However, there are cases that damping might be violently decreased as in the case of the explosive flutter. Hence flutter might be encountered causing severe damage to the aircraft. Accordingly, such tests are also accompanied by numerous numerical analyses, wind tunnel and ground testing in order to avoid bringing the tested aircraft too close to the flutter boundary [1].

Various flight-test data-analysis methods are available for application in on- and off-line manners to identify the flutter conditions. Examples of the used approaches are: damping extrapolation [2] , envelope function [3], the Zimmerman-Weissenburger flutter margin [4], the model-based flutterometer method [5], and using a discrete-time autoregressive moving average (ARMA) model [6]. As being at flutter conditions might have catastrophic results, all the approaches are based, in this way or another, on extrapolating for the flutter conditions while staying at safe conditions, which makes the tests expensive, time consuming and risky.

On the contrary, the Parametric Flutter Margin (PFM) methodology [7] is based on analysing frequency-response functions (FRFs) of a stabilized system, which allows us to identify flutter positively without exceeding the pre-determined safe vibration levels. It is anticipated that the PFM methodology will be very instrumental in the design of future flutter-test campaigns improving their safety and reduce the time and effort required to ensure the flight envelope is indeed flutter free.

Karpel and Roizner [8] proposed a novel method for finding the flutter boundary experimentally based on their numerical PFM method [7]. The experimental PFM mitigates some of the deficiencies of the currently established methods, namely the need to approach the flutter boundary cautiously, and that the flutter boundary is never positively identified. The PFM method is based on the idea that the stability point of an aeroelastic system can be offset by adding a stabilising element. In the case of wing flutter, such a stabilising element could be an added mass at the leading edge of the wing tip. Such an augmented system is then subjected to harmonic excitation in order to obtain the FRF of the stabilising element, for instance the acceleration of the added mass which is then analysed for gain margin at phase-cross-over frequency. The flutter boundary of the original system excluding the added stabilising mass is reached when the gain margin of the stabilising element equals 0 dB. The FRF analysis is repeated at various flight conditions in order to obtain the gain margin vs. flight speed characteristics. The flutter speed is read from the graph at 0dB. Details on theoretical foundation of the PFM method and its formulation are provided in [7] while the key equations and their application related to this experiment are outlined in this paper.

It is worth pointing out that PFM method allows for the flutter boundary identification of the original system excluding the added mass without the need to approach the stability boundary of the augmented system because the system is stable at the original system flutter speed. This greatly reduces the risk of such experimental efforts.

The contribution to the state of the art of the current manuscript is a proof of concept and validation of the proposed PFM method using a typical wing section with pitch and plunge degree of freedom (DOF) mounted in the wind tunnel. The paper is organized as follows: in Sec. 2 the mathematical formulation of the 2DOF aeroelastic system along with its PFM implementation related to the experiment is presented, Sec. 3 describes the experimental set up and the testing procedure. The results are shown in Sec. 4, and the conclusions of this work are given in Sec. 5.

2 THEORETICAL MODEL OF THE AEROELASTIC SYSTEM

The mathematical formulation of the 2DOF airfoil along with its PFM implementation relevant to this experiment is presented in this Section. The mathematical model was used for three main purposes. The first purpose was to evaluate the experimental setup in order to obtain the aeroelastic instability at a velocity within the wind tunnel limits. The second was to size and position the stabilizing weight such that the flutter velocity was increased by at least 15%, and the third reason was the comparison with the experimental results. It has to be stressed however, that the experimental PFM method or its results do not depend on the mathematical model. The experimental PFM method is not a model-based method.

First the governing equations of motion are presented, followed by the presentation of the PFM methodology.

2.1 Equation of motion

The experimental aeroelastic system was modelled using a typical section with pitch and heave DOFs as depicted in Figure 1. The airfoil of chord length $2b$, mass m_0 and moment of inertia

J_0 expressed around the centre of gravity at C_0 is hinged at the point P. Additionally, m^* represents all the additional support mass, such as the mass of the pitching mechanism, supported by the leaf springs governing the heaving motion. This mass is involved in the heave motion only, and does not contribute to the overall moment of inertia involved in the pitching motion. Stiffness and damping characteristics of the pitch and heave DOFs are presented by k_θ and d_θ, and k_h and d_h, respectively. Lift L, and aerodynamic moment $M_{c/4}$ are assumed to act at the quarter-chord point Q. The external excitation force F_s is applied at the same location as the stabilising mass at point C_s. The points P and C_0 are expressed in terms of airfoil half chord b and non-dimensional parameters a and e_0 that can assume values between [-1, 1], with -1 being the airfoil leading edge and 1 the airfoil trailing edge. The response of the section to L, F_s, and $M_{c/4}$ is governed by the following equation of motion:

$$\begin{bmatrix} 1+\mu_* & x_0 \\ x_0 & r^2 \end{bmatrix} \begin{Bmatrix} \ddot{\xi} \\ \ddot{\theta} \end{Bmatrix} + \begin{bmatrix} \eta_\xi & 0 \\ 0 & \eta_\theta \end{bmatrix} \begin{Bmatrix} \dot{\xi} \\ \dot{\theta} \end{Bmatrix} + \begin{bmatrix} \omega_\xi^2 & 0 \\ 0 & r^2\,\omega_\theta^2 \end{bmatrix} \begin{Bmatrix} \xi \\ \theta \end{Bmatrix} = \begin{Bmatrix} \chi_\xi \\ \chi_\theta \end{Bmatrix} \tag{1}$$

where $\xi = h/b$ and θ represent dimensionless heave and pitch DOFs. $x_0 = e_0 - a$ is the eccentricity parameter of the airfoil section. $r^2 = (J_0 + m_0 x_0^2 b^2)/m_0 b^2$ represents the dimensionless radius of gyration of the section about the pivot point P. $\mu_* = m^*/m_0$ is the ratio between the support mass and the section mass. $\eta_\xi = d_h/m_0 b$ and $\eta_\theta = d_\theta/m_0 b^2$, $\omega_\xi = \sqrt{k_h/m_0}$ and $\omega_\theta = \sqrt{k_\theta/(J_0 + m_0 x_0^2 b^2)}$ are the normalised damping coefficients and the circular frequencies of the heave and pitch DOF, respectively. Finally, χ_ξ and χ_θ are the forces of the corresponding DOFs given as:

$$\begin{aligned} \chi_\xi &= \frac{1}{m_0 b}(-L + F_s) \\ \chi_\theta &= \frac{1}{m_0 b^2}\left(M_{c/4} + \left(\frac{1}{2} + a\right) bL + x_s b F_s\right) \end{aligned} \tag{2}$$

Relative thickness of the section's airfoil is 12%, the excitation force $F_s = \hat{F}_s e^{i\omega t}$ is harmonic, hence unsteady thin-airfoil theory and harmonic motion of the section are valid assumptions. Consequently, L and $M_{c/4}$ can be expressed using the Theodorsen theory [9] as:

$$\begin{aligned} L &= 2\pi\rho v_\infty b^2 C(k)\left(\dot{\xi} + \frac{v_0}{b}\theta + \left(\frac{1}{2} - a\right)\dot{\theta}\right) \\ &\quad + \pi\rho b^3\left(\ddot{\xi} + \frac{v_0}{b}\dot{\theta} - a\ddot{\theta}\right) \\ M_{c/4} &= -\pi\rho b^4\left(\frac{1}{2}\ddot{\xi} + \frac{v_0}{b}\dot{\theta} + \left(\frac{1}{8} - \frac{a}{2}\right)\ddot{\theta}\right) \end{aligned} \tag{3}$$

where $C(k)$ represents the Theodorsen function, k the reduced frequency, v_0 the airstream velocity and ρ the air density.

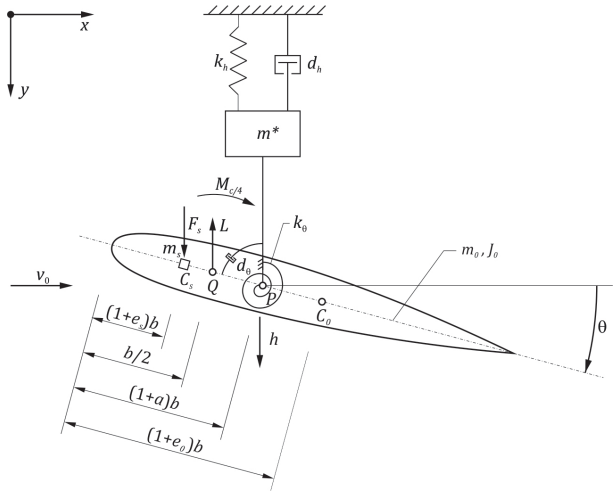

Figure 1: Typical section with pitch and heave DOF

2.2 Parametric flutter margin method

The implementation of the PFM method [7] for identifying flutter of the 2DOF airfoil using a stabilizing mass is briefly outlined in this subsection. The flutter equation is obtained by transforming Eq. (1) to frequency domain (FD) and by setting the external excitation to zero. Accordingly, Eq. (1) becomes:

$$[A(i\omega)]\{\zeta(i\omega)\} = \{0\} \tag{4}$$

where $\{\zeta(i\omega)\} = \{\xi, \theta\}^T$, and the system matrix $[A(i\omega)]$ contains the structural mass, damping and stiffness matrices, and the frequency-depended aerodynamic coefficient matrix. Flutter conditions are defined mathematically as the flight parameters at which Eq. (4) yields a non-trivial solution. Common flutter methods such as the p-k [10] and k-methods [11] are based on searching, in this way or another, for the flight conditions at which $|A(i\omega)| = 0$.

The PFM procedure, on the other hand, searches for the flutter boundary using FRFs due to the excitation introduced in the right side of Eq. (4). The response of the original system approaches infinity at the stability boundary, FRFs are therefore calculated with $[A(i\omega)]$ modified to include the effect of a stabilizing parameter. In our case, a stabilizing mass represented by $\mu_s = m_s/m_0$ located at C_s is used as a stabilizing element. The flutter conditions are found by measuring the acceleration at C_s, represented by y_f. The equation of motion with the added stabilizing element is

$$\begin{gathered}\left[A(i\omega) + \mu_s\{B_f\}[C(i\omega)]\right]\{\zeta(i\omega)\} = \{B_f\}u_f(i\omega) \\ y_f(i\omega) = \left[C_f(i\omega)\right]\{\zeta(i\omega)\}\end{gathered} \tag{5}$$

where u_f is the excitation input, which represents the amplitude of the excitation applied at C_s, distributed to the system through $\{B_f\} = \{1, x_s\}^T$, and $\left[C_f(i\omega)\right] = -\omega^2[1\ x_s]$ defines the acceleration sensor. For a given $u_f(i\omega)$ one can solve Eq. (5) for $\{\zeta(i\omega)\}$ and $y_f(i\omega)$ at all stable flight points of the stabilised aeroelastic system, including at the nominal flutter point of the original system which is now stable. Furthermore, the flight conditions and the excitation frequency for which

$$u_f(i\omega_f) = \mu_s y_f(i\omega_f) \tag{6}$$

is satisfied must reflect the flutter-onset conditions because the added terms vanish and Eq. (5) reduces back to the homogeneous Eq. (4). The calculated $\{\zeta(i\omega_f)\}$ is the nontrivial solution of Eq. (2), namely the flutter mode. At other points, the ratio $y_f(i\omega_f)/u_f(i\omega_f)$ define the flutter margins with respect to μ_s.

The PFM flutter analysis starts with calculating $y_f(i\omega)$ in response to $u_f(i\omega)$. To find the flutter on-set conditions, in which Eq. (6) is satisfied in both magnitude and phase, response functions are first generated at various velocities and constant altitude, and Bode plots are generated in terms of real-valued gain and phase functions:

$$\begin{aligned} Y_f(\omega) &= 20\,log\left|\mu_s y_f(i\omega)/u_f(i\omega)\right| \\ \Phi_f(\omega) &= \angle\left(\mu_s y_f(i\omega)/u_f(i\omega)\right) \end{aligned} \tag{7}$$

These plots are then used for calculating the phase cross-over gains $Y_f(\omega_{pco})$, where ω_{pco} is a phase-cross-over frequency at which $\Phi_f(\omega_{pco}) = \pm 360n$. The system is neutrally stable at the interpolated velocity v_f where $Y_f(\omega_{pco}) = 0\text{dB}$. The flutter frequency $\omega_f = \omega_{pco}$ and the complex flutter mode is $\{\zeta_f(i\omega_{pco})\}$.

3 EXPERIMENT

3.1 Experimental setup

The experimental setup developed by Gjerek et al. [12] was used in this work as it has a well-defined pitch and heave DOFs with the possibility of adjusting the stiffness of each DOF individually. In addition, other important parameters governing aeroelastic response of the airfoil, such as pitch axis, centre of gravity location, mass and moment of inertia, can be varied. As a result, various aeroelastic configurations can be easily studied and the apparatus can be tailored to meet the requirements of the wind tunnel and those of the PFM method. The apparatus is shown in Figure 2.

The heave mechanism consists of two pairs of cantilever leaf springs at the top and bottom of the apparatus as shown in Figure 2a. The heave stiffness, k_h, is adjusted by changing the length of the springs. The heave mechanism also supports the pitch mechanism, which governs the torsional stiffness and provides support to the rigid airfoil. The pitch mechanism is shown in more detail in Figure 2b. Torsional stiffness is introduced by a pair of preloaded extension springs attached to the pulley which is mounted on the axle of the rigid airfoil. Torsional stiffness can be adjusted by changing the extensional springs or the diameter of the pulley. Both mechanisms are placed outside the test section not to obstruct the airflow.

The stabilising weight is mounted by a pair of aluminium rods attached to the airfoil's axle outside the test section as shown in Figure 2c. Mass of the stabilising weight as well as its distance from the rotational axis can be adjusted in order to achieve sufficient increase of the flutter speed for safe application of the PFM method.

Both pitch and heave DOF were limited with physical motion stoppers. Motion stoppers allowed direct measurement of the flutter onset conditions by increasing the air velocity until flutter was observed.

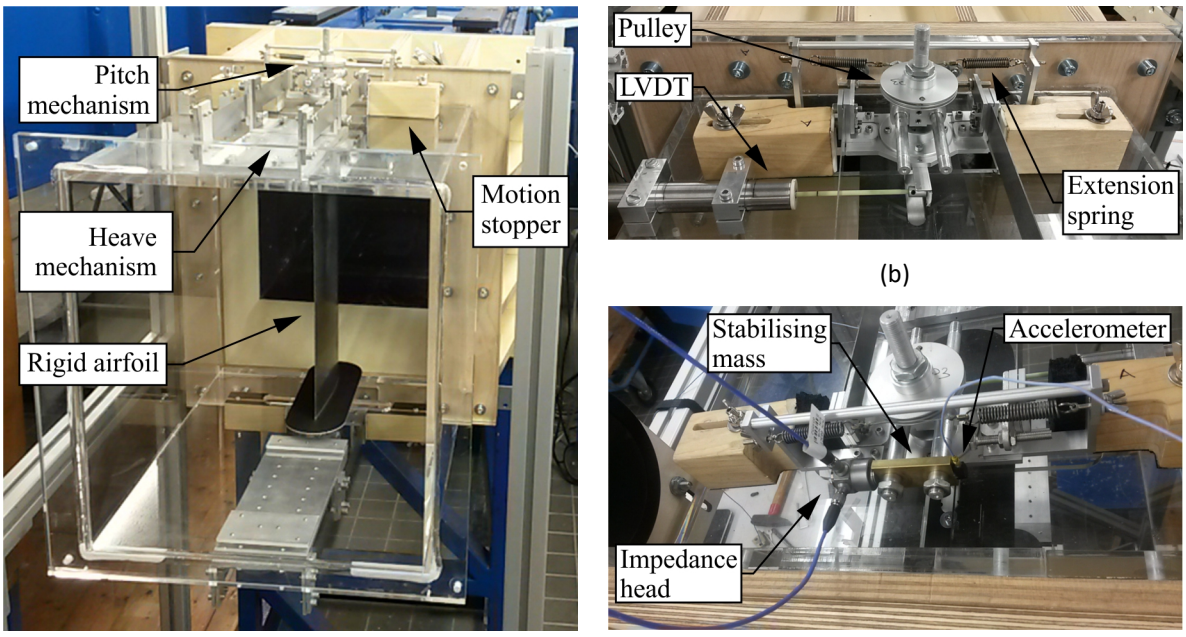

Figure 2: Experimental setup: (a) overview, (b) pitch mechanism, (c) stabilising mass with impedance head and accelerometer

Based on the preliminary investigation two configurations were selected which physical properties are summarised in Table 1. The listed physical properties are already updated with the results from the system identification tests. The main difference between the two selected configurations is the torsional stiffness k_θ, which significantly alters the flutter and divergence boundary of the experimental setup. Torsional stiffness was set to $1.65\,\mathrm{Nm/rad}$ and $3.14\,\mathrm{Nm/rad}$ for configuration 1 and configuration 2 respectively.

3.2 Instrumentation and excitation

The aeroelastic response of the airfoil was monitored using displacement and rotation sensors, an impedance head and a set of accelerometers. The airfoil motion was measured using a linear and rotational variable differential transformer, LVDT and RVDT, attached to the airfoil's axle. Placement of the sensors, their type and orientation are indicated in Figure 3.

The PFM method requires to apply the force and to measure the resulting acceleration at the stabilising mass location. Accordingly, an impedance head was used and mounted directly on the stabilising weight as depicted in Figure 2c. Therewith the gain, Y_f, and phase, Φ_f, as defined by Eq. (7) can be directly measured. Redundant accelerometers, a_1 and a_2, were mounted on the airfoil's axle and on the other side of the stabilising weight in order to provide control measurements.

Parameter	Unit	Quantity
airfoil	[-]	NACA 0012
chord × span, $2b \times s$	$[\mathrm{m}^2]$	0.16×0.36
airfoil mass, m_0	[kg]	0.622
heave mass, m^*	[kg]	0.441
moment of inertia, j_0	$[\mathrm{kg\,m}^2]$	$1.92 \cdot 10^{-3}$
axis of rotation, $(1+a)b$	[m]	0.064
CG, $(1+e_0)b$	[m]	0.067
heave stiffness, k_h	[N/m]	710
heave damping, D_h	[Ns/m]	1.5
pitch stiffness, k_θ	[Nm/rad]	1.65, 3.14†
pitch damping, D_θ	[Nms/rad]	0.0066, 0.0035†

†values pertinent to configuration 1 and 2 respectively.

Table 1: Physical properties of the experimental setup for configuration 1 and 2

Mass of the installed sensors has to be properly accounted for. While the mass of the sensors attached directly to the airfoil is negligible relative to the airfoil's mass, the mass of the sensors attached to the stabilising weight is not. The impedance head and the control accelerometer with their pertinent cabling contribute $\sim 40\%$ to the overall stabilising mass. These masses were hence added to the total stabilising mass used in the determination of the FRFs.

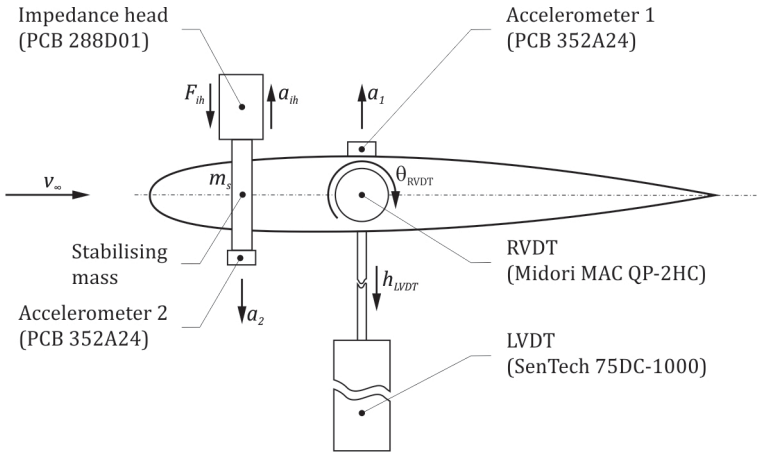

Figure 3: Instrumentation of the aeroelastic system

The excitation signal, $u_f(t)$, measured by the impedance head was an impulse force provided by a hit of a hammer.

3.3 Testing procedure

Both of the selected configurations were tested for flutter while configuration 1 was also tested for divergence. For each case two tests were performed using a conventional approach and the PFM method. This way the aeroelastic stability boundary obtained by means of the PFM method could be directly compared to the flutter or divergence onset conditions observed on the original, non-augmented aeroelastic system.

3.3.1 Flutter test

Flutter properties of each configuration were first investigated by monitoring the response of the original aeroelastic system to a small perturbation while slowly increasing the airstream

velocity. The system was excited manually by exerting a short force on the model such that both heave and plunge DOF were excited simultaneously. The airstream velocity was increased until the flutter instability set in.

In the next step, the aeroelastic system was augmented by adding the stabilising mass. Again, the same procedure was applied in order to establish the flutter properties of the augmented system and demonstrate that the augmented system remains stable at the flutter conditions of the original system.

For applying the PFM methodology, FRFs at selected airstream velocities, v_0, were determined by recording the time signal of the excitation force and the stabilising weight's acceleration. The measured signals were converted to the frequency domain using the fast Fourier transform (FFT) and the FRF was constructed as:

$$H(\omega; v_0) = \frac{m_s a_s(\omega; v_0)}{F_s(\omega;\ v_0)} \tag{8}$$

where a_S is the acceleration of the stabilising weight measured either by the impedance head or the accelerometer 2 as depicted in Figure 3. m_s and F_s are the mass of the stabilising weight and the external force as shown in Figure 2. F_s was applied directly to the stabilising mass and measured by the impedance head.

After obtaining sufficient FRFs over a range of v_0 the methodology outlined in section 2.2 is used. The Bode plots are generated and the experimental phase-cross-over frequencies and corresponding gains for each v_0 are determined. These in turn can be plotted as a function of v_0 which allows to determine the flutter velocity and frequency, which equal to the airstream velocity and phase-cross-over frequency at which the phase-cross-over gain equals 0dB.

The excitation force can be applied in various ways, for example, by using an electromechanical shaker or an impedance hammer, as long as it contains sufficient energy to excite the aeroelastic modes involved in the flutter mechanism. In the current experiment, it was decided to use a regular hammer since it didn't constrain the motion of the aeroelastic system after applying the force.

3.3.2 Divergence test

Similar to the flutter investigation, divergence was first determined in a conventional way followed by the application of the PFM method.

During the conventional investigation, configuration 1 of the aeroelastic system was used. In addition, enough stabilising mass was added to the aeroelastic system such that the divergence would set in before flutter. Again, the airstream velocity was gradually increased and the system response in terms of pitch and heave displacement to a small perturbation was measured. An example of such a measurement is shown in Figure 11a. The airstream velocity was increased until a sharp increase in the measured displacements was observed.

The PFM method is performed as follows. First, the aeroelastic system is stabilised by adding a stabilising torsional spring of stiffness, k_θ^s, to the pitch DOF in order to offset the divergence onset to a higher v_0. Then a constant torque, M_0, is applied to the pitch DOF and θ is measured while v_0 is increased. The original aeroelastic system diverges at v_D when the torsional deflection of the augmented aeroelastic system satisfies the following condition:

$$\theta(v_D) = \theta^s = \left.\frac{M_0}{k_\theta^s}\right|_{v_0=0m/s} \tag{9}$$

where θ^s represents the torsional deflection of the stabilising torsional spring under applied torque M_0, and wind-off conditions, $v_0 = 0$.

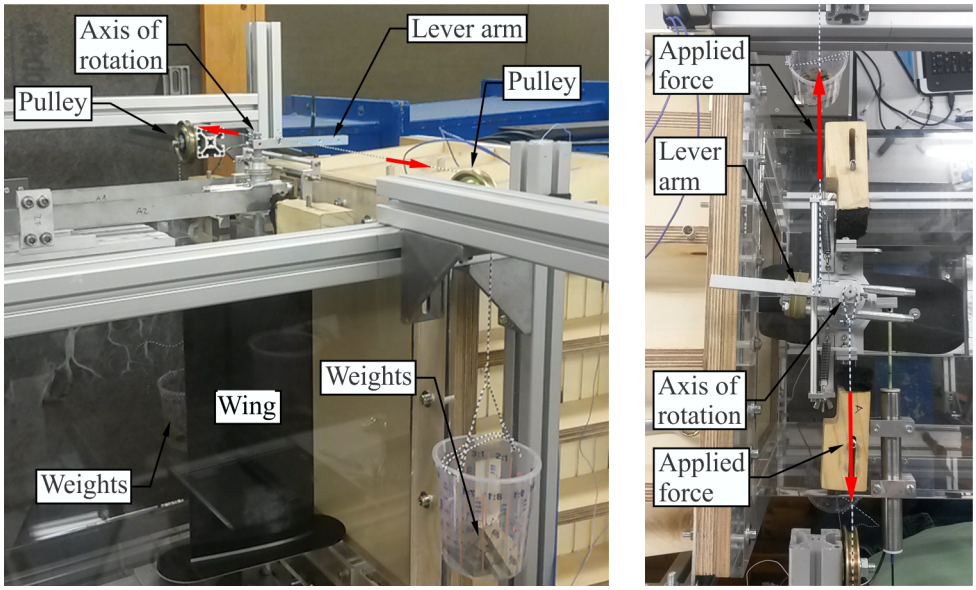

(a) (b)

Figure 4: Divergence setup: (a) overview, and (b) top view

Torsional stiffness, k_θ, of the aeroelastic system is governed by the pulley-spring mechanism, shown in Figure 2b, as:

$$k_\theta = 2k_s r_p^2 \tag{10}$$

where k_s represents the stiffness of the extensional springs and r_p represents the pulley radius. Since a pulley can be easily exchanged, it was decided to introduce the stabilising torsional stiffness k_θ^s by swapping the pulley in the original aeroelastic system with a second pulley of a larger radius, r_{p1}, such that:

$$k_{\theta 1} = k_\theta + k_\theta^s \tag{11}$$

In order to be able to measure θ^s a third pulley of radius r_p^s was machined such that

$$k_\theta^s = 2k_s r_p^{s2} \tag{12}$$

As a result, the actual divergence test was performed in the following order. First, the pulley of radius r_p^s was installed and θ^s at M_0 and $v_0 = 0\text{m/s}$ was measured. Then the pulley of radius r_{p1} was installed and v_0 was increased until the condition expressed by Eq. (9) was met.

The torque M_0 was applied by a force couple exerted by weights hung from the pulley as shown in Figure 4a. A top view of the lever arm and the cable attachment is shown in Figure 4b.

4 RESULTS AND DISCUSSION

Experimental results obtained during the wind tunnel campaign are presented and discussed in this section. System identification results are presented first, followed by the conventional and the PFM flutter tests, the divergence results are discussed in the end.

4.1 System identification

A system identification was performed as part of the flutter tests when the aeroelastic system was fully assembled and mounted in the wind tunnel. This way stiffness and damping properties could be determined in order to update the theoretical model presented in section 2.

System identification was performed by fitting the transfer function expressed by Eq. (7) to the measured response. Results for both configuration 1 and 2 are shown in Figure 5. The identified properties are included in Table 1. In general, good agreement between the measurements and the fitted response can be observed, especially in the range of frequencies that are interesting from the flutter investigation point of view, around 4.5Hz for configuration 1 and 5.1Hz for configuration 2.

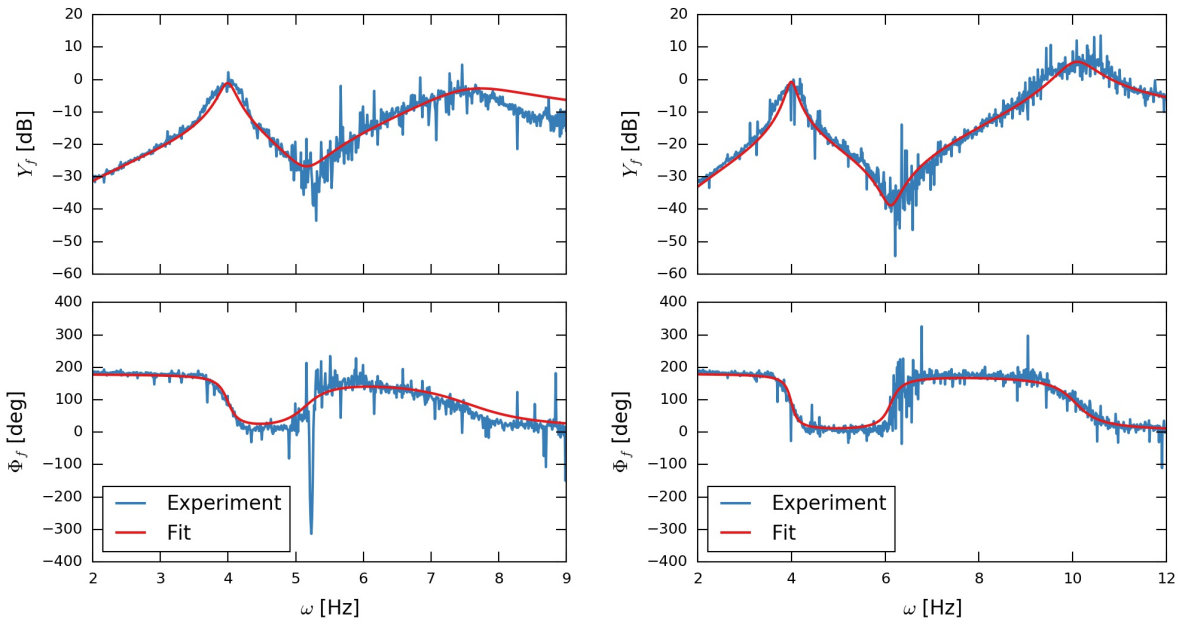

Figure 5: System identification: (a) configuration 1, and (b) configuration 2

4.2 Flutter

Flutter conditions were first identified for the original, non-augmented system following the procedure outlined in section 3.3.1. Heave and pitch response to a small perturbation at two consecutive airstream velocities are shown for both of the investigated configurations in Figure 6. In the case of configuration 1, a converging response is observed at $v_0 = 15.2\text{m/s}$ and a diverging response at $v_0 = 15.4\text{m/s}$. Hence it was concluded that the original aeroelastic system in configuration 1 would flutter at 15.3m/s.

In the case of configuration 2, a converging response is observed at $v_0 = 22.5\text{m/s}$ and a constant amplitude response at $v_0 = 22.7\text{m/s}$, which indicates that the damping is virtually 0 and that the system is at the flutter boundary. Hence it was concluded that the flutter speed pertinent to configuration 2 is at 22.7m/s.

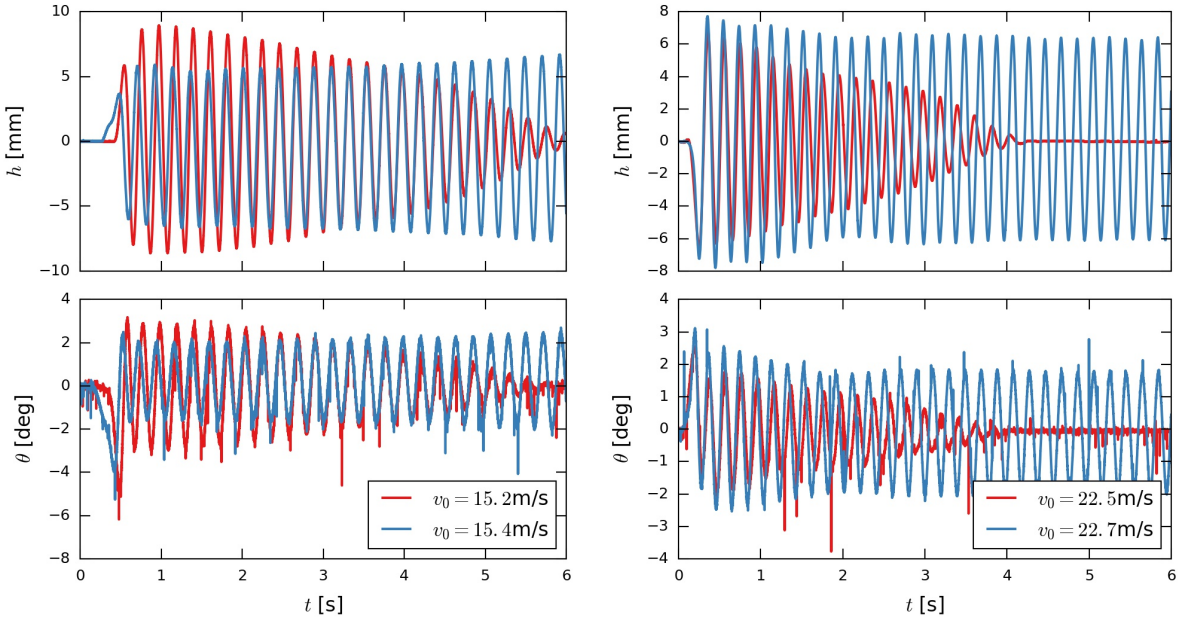

Figure 6: Flutter response: (a) configuration 1, and (b) configuration 2

Measurement of the FRFs defined by Eq. (7) lies at the heart of the PFM method. The measured FRFs at three different airstream velocities are shown in Figures 7a and 8a for each configuration respectively. The experimental results are shown as dotted lines. Despite the fact that these results were obtained by averaging over the response measured by both the impedance head and the control accelerometer, a_2, and over several excitation responses, one can still observe some noise present in the signal which renders the determination of the ω_{pco}, and the corresponding gain, $Y_f(\omega_{pco})$, more difficult. Therefore, it was decided to fit a transfer function to the measurements as depicted by the full lines in Figures 7a and 8a over a selected range of frequencies around the ω_{pco}. Nevertheless, it is clear from the experimental result that once v_0 exceeds the flutter speed of the original system, $Y_f(\omega_{pco})$ exceeds 0dB.

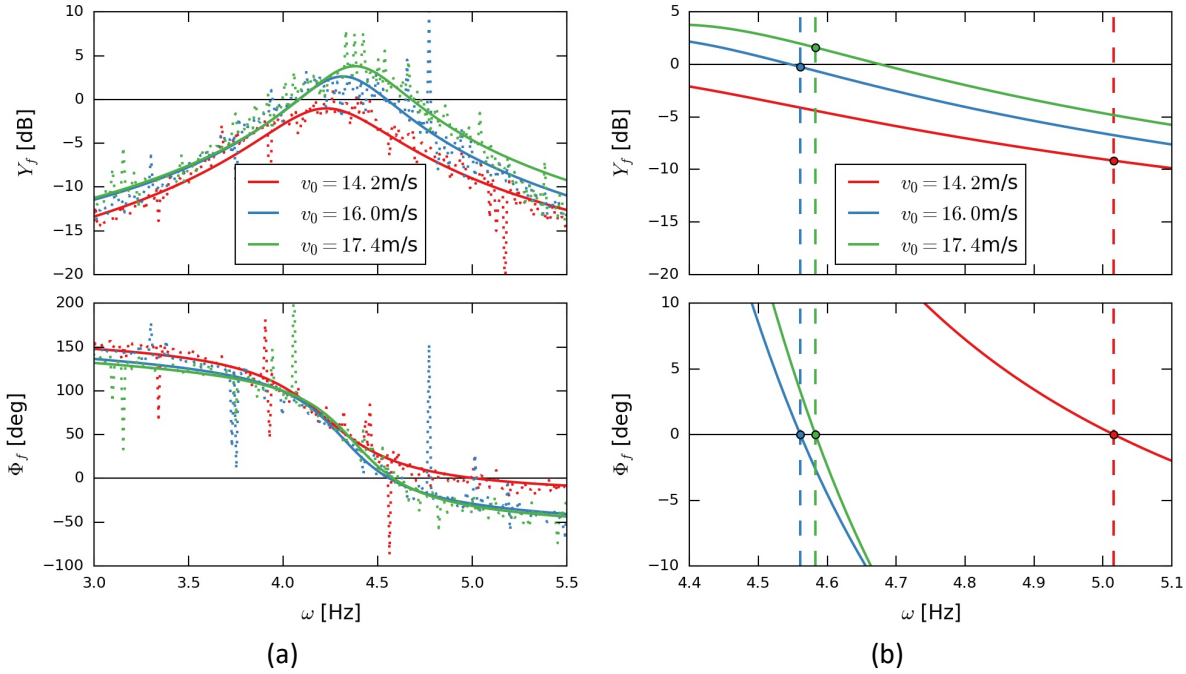

Figure 7: (a) Configuration 1 Bode plots, and (b) zoom-in region around phase-cross-over frequency

A transfer function used for fitting had two poles and two zeros. Therewith smooth continuous Bode plots were obtained that were used for determination of the ω_{pco} and $Y_f(\omega_{pco})$. It is important to understand that the transfer functions were used as an "averaging" tool in order to obtain smooth response close to ω_{pco}, and were only required to match the measured response in the neighbourhood of ω_{pco} frequencies: around 4.5Hz for the first configuration and around 5.1Hz for the second configuration.

ω_{pco} and $Y_f(\omega_{pco})$ are determined in two steps by inspecting Figure 7b or 8b. First, ω_{pco} is defined by the crossing of the Φ_f curve with 0deg line as indicated by the round markers in the bottom subplot of the two figures. Next, following the vertical dashed line a crossing with the Y_f curve is found which defines the $Y_f(\omega_{pco})$. The corresponding crossings are marked by the round markers in the top subplot of Figure 7b or 8b. The procedure is repeated for every measured v_0.

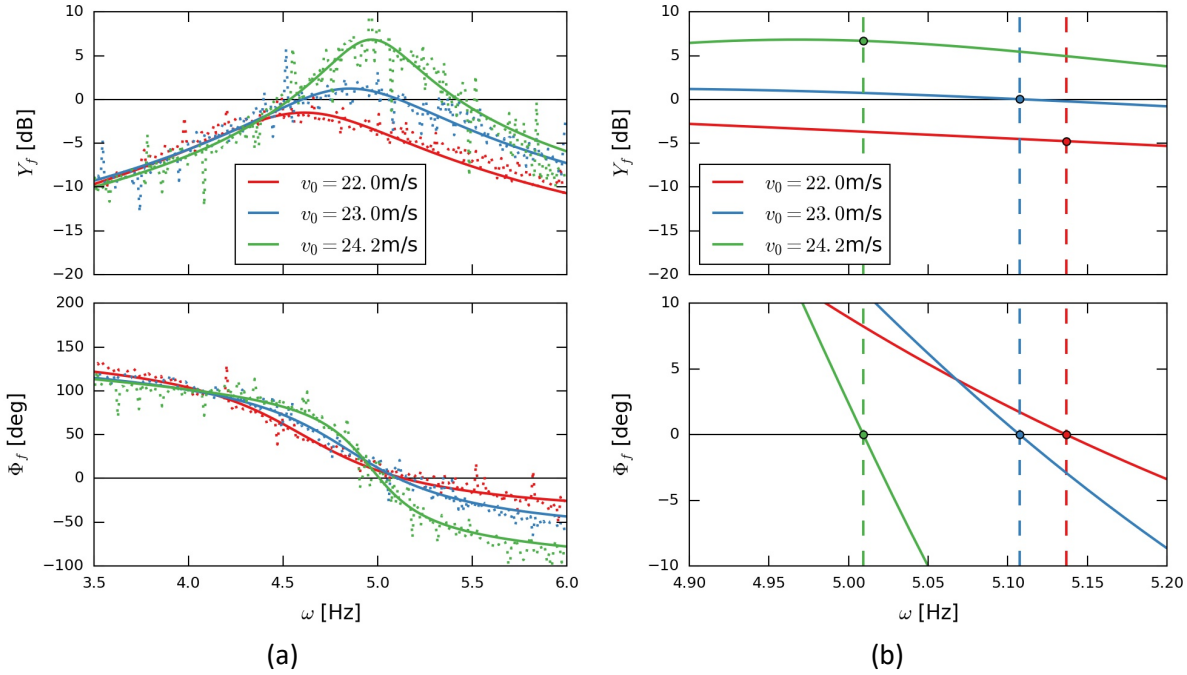

Figure 8: (a) Configuration 2 Bode plots, and (b) zoom-in region around phase-cross-over frequency

The measured ω_{pco} and $Y_f(\omega_{pco})$ are collected in the parametric flutter margin plots (PFM plots) as a function of airstream velocity. $Y_f(\omega_{pco})$ gains are expressed in terms of PFM, which essentially represents the gain margin with respect to 0dB. The PFM plots pertinent to configurations 1 and 2 are shown in Figures 9 and 10. Flutter conditions found by the conventional approach are added for the sake of comparison. These results are shown as green rectangular markers.

Flutter conditions are then found from the PFM plots. The flutter velocity, v_f, is determined by finding the crossing of the PFM line with the 0dB line. The corresponding v_f are indicated by the vertical dashed lines in the top subplot of Figure 9 or 10. The flutter frequency, ω_f is then found by following the dashed line until a crossing with the ω_{pco} curve in the bottom subplot of the two figures is reached.

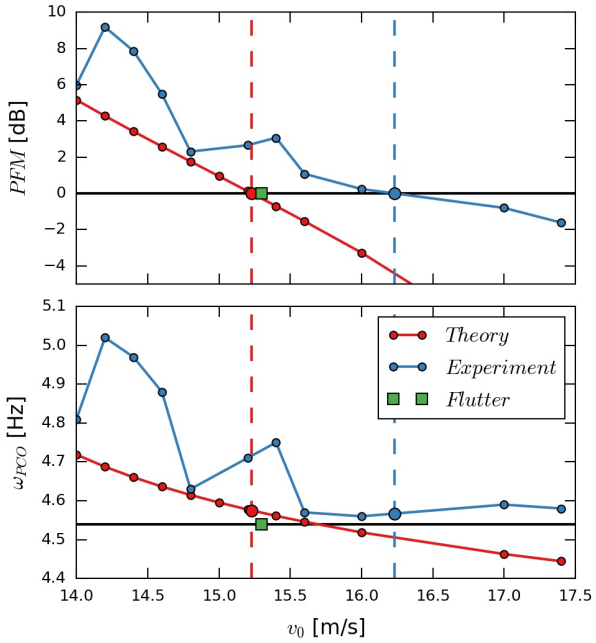

Figure 9: PFM plot for configuration 1

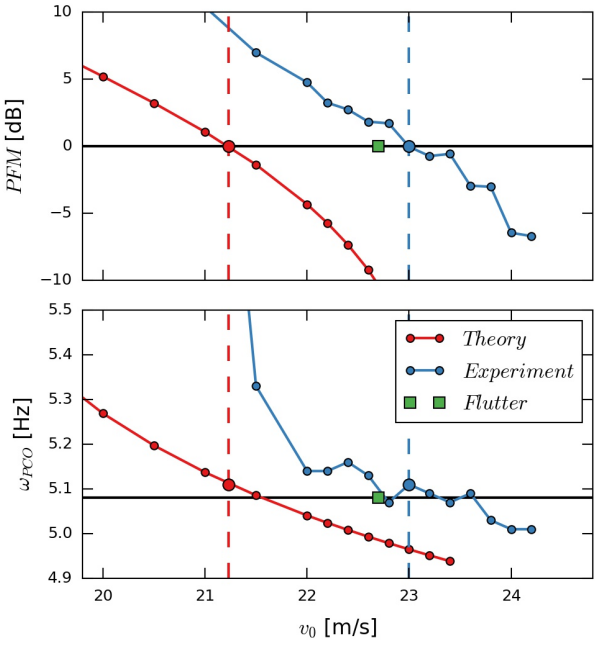

Figure 10: PFM plot for configuration 2

Summary of all the flutter results is provided by Table 2. One can observe that the agreement between all methods, the conventional flutter test, the PFM test and theoretical PFM method is very good. The observed difference in predicted flutter velocity between the conventional and the PFM test is 6% in the case of configuration 1 and 1% in the case of configuration 2. The agreement is even better as far as the predicted flutter frequency is concerned. In this case the observed difference is about 0.5% for both configuration 1 and 2. Furthermore, the differences in the case of the theoretical PFM model are of the same order of magnitude as those observed in the comparison between the conventional flutter test and the PFM test.

	Parameter	Flutter	PFM (exp.)	PFM (thry.)
Configuration 1	v_f [m/s]	15.3	16.2 (1.06)†	15.2 (0.99)†
	ω_f[Hz]	4.54	4.56 (1.004)†	4.57 (1.007)†
Configuration 2	v_f [m/s]	22.7	23.0 (1.01)†	21.2 (0.94)†
	ω_f [Hz]	5.08	5.11 (1.006)†	5.11 (1.006)†

†relative to the results reported as Flutter

Table 2: Flutter results summary

4.3 Divergence

The results of the divergence measurements using both the conventional approach and the PFM method are presented in this section. Divergence was investigated for the first configuration of the aeroelastic system.

Figure 11 shows the measurements obtained using the conventional approach, as described in section 3.3.2. A typical time record of the system response in heave and pitch DOF due to small perturbation is shown in Figure 11a. One can observe that after the transient effects die out the system remains in a new equilibrium position having increased heave and pitch displacement, h and θ. The difference Δh and $\Delta\theta$ was determined from the measurements and plotted against v_0 as shown in Figure 11b. Both Δh and $\Delta\theta$ increase in magnitude with increasing v_0. Moreover, as the divergence speed is approached the increase in Δh and $\Delta\theta$ rapidly increases as well. Such a rapid increase, especially in the pitch DOF is observed at $19\mathrm{m/s}$. $\Delta\theta$ increased more than three-fold due to a speed increment of $0.2\mathrm{m/s}$. $v_0 = 19\mathrm{m/s}$ is therefore considered to mark the divergence onset velocity.

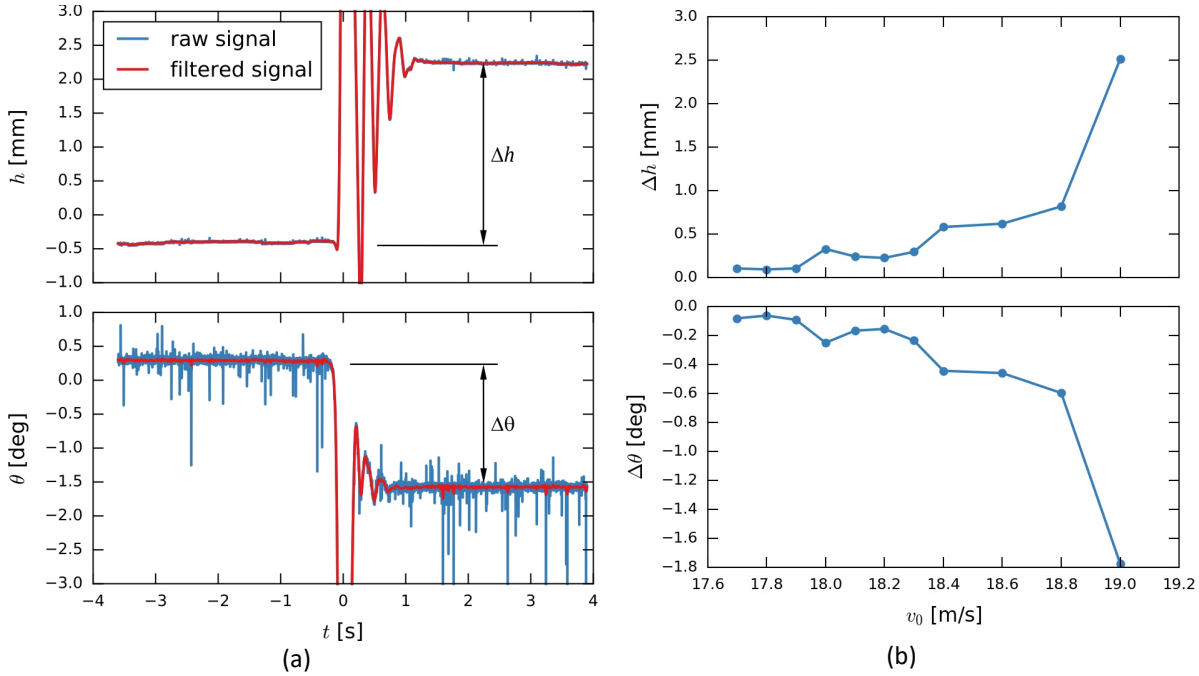

Figure 11: Deflection measurements at $19\mathrm{m/s}$, (a), and heave and pitch DOF displacement as a function of velocity, (b)

The PFM results are presented in Figure 12. A reference measurement used to investigate the airfoil alignment with the airstream is shown by the green line. The measured deflections are very small, less than 4% of those measured during the PFM experiment shown by the red line, over the entire range of the investigated airstream velocities. Hence, one can conclude that the

wing was well aligned with the airstream and that negligible deflections due to the initial angle of attack can be expected.

The actual PFM experiment is represented by a red line. Expectedly as v_0 is increased both $\Delta\theta$ and Δh increase as the wing assumes a new aeroelastic equilibrium. $\Delta\theta$ reaches the value of θ^s of Eq. (9), indicated by the red dotted line, at 19.4 m/s, which marks the divergence onset velocity. The divergence velocity obtained with the conventional method is indicated by the orange vertical line for the sake of comparison. The two methods show very good agreement, with the difference of only 1%.

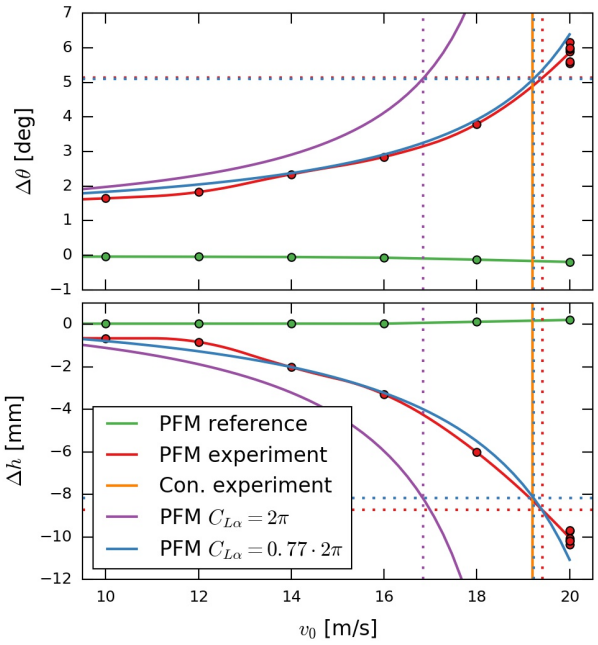

Figure 12: PFM divergence results for configuration 1

Numerical PFM results, depicted in purple and blue, are also shown for the sake of comparison. Results depicted in purple were obtained using a numerical model assuming an infinite wing with a lift slope $C_{L\alpha} = 2\pi$. Results depicted in blue were obtained by correcting the $C_{L\alpha}$ coefficient for the finite span effect. The improvement is significant. The difference with respect to the experimental results is reduced from 9% to less than a 1%.

The correction is based on the Δh measurement from the PFM experiment shown in Figure 12. In connection with the heave stiffness of the aeroelastic system the lift generated by the wing can be estimated. The results are shown in Figure 13. The obtained results are compared to the theoretical results obtained using $C_{L\alpha} = 2\pi$ and $C_{L\alpha} = 2\pi/(1 + 2/AR)$, with $AR = 2$ representing the aspect ratio of the wing. It is clear that despite mounting the endplates on the wing, finite span effects are still present and have significant effect on the $C_{L\alpha}$.

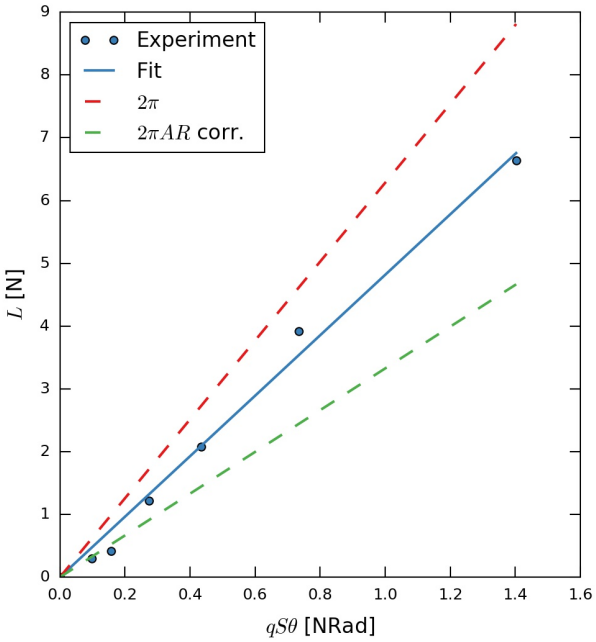

Figure 13: Finite span lift correction for configuration 1

5 CONCLUSIONS

A novel method for safe experimental identification of aeroelastic instabilities based on Parametric Flutter Margins has been demonstrated by successfully predicting flutter as well as divergence onset of an aeroelastic model mounted in the wind tunnel. Performing the PFM tests by adding stabilizing weight or spring, the instability points are positively identified without risking the model's structural integrity.

Two different configurations of the aeroelastic model have been tested for flutter. Very good to excellent agreement between the conventional flutter test and the PFM method has been achieved. The difference in predicted flutter velocity and flutter frequency were less than 6% and less than 0.4% respectively for configuration 1. The observed differences were even smaller for configuration 2, less than 1% and less than 0.6%. Moreover, similar differences were observed in the comparison with the theoretical PFM method.

Aeroelastic system in configuration 1 was also tested for divergence. Initially, a reasonable agreement between the conventional approach and the PFM method was observed, with a 9% difference between the two. However, after the PFM measurements were corrected for the finite wing effects the agreement was significantly improved. As a result, the observed difference was reduced to less than 1%.

A unique feature of the PFM method, that an instability boundary can be safely crossed without risking the aeroelastic model, has been demonstrated as well.

Due to its accuracy and unique properties, the PFM method marks an important contribution to the state of the art in testing for aeroelastic instabilities, with significant potential for improvement in the safety of flutter flight tests.

6 ACKNOWLEDGMENT

The authors would like express their gratitude to Dr. Bojan Gjerek for sharing his aeroelastic apparatus with them for conducting the aeroelastic experiments presented in this paper.

The authors would also like to thank Bruce Le Blanc for his advice and help with instrumentation of the aeroelastic system.

7 REFERENCES

[1] D. H. Hodges and G. A. Pierce, *Introduction to structural dynamics and aeroelasticity*, 2nd ed. New York: Cambridge University Press, 2011.

[2] M. W. Kehoe, 'A historical overview of flight flutter testing', *NASA TM-4720*, Oct. 1995.

[3] J. E. Cooper, P. R. Emmett, J. R. Wright, and M. J. Schofield, 'Envelope function - A tool for analyzing flutter data', *J. Aircr.*, vol. 30, no. 5, pp. 785–790, 1993.

[4] J. T. Weissenburger and N. H. Zimmerman, 'Prediction of flutter onset speed based on flight testing at subcritical speeds', *J. Aircr.*, vol. 1, no. 4, pp. 190–202, 1964.

[5] R. Lind and M. Brenner, 'Flutterometer: An On-Line Tool to Predict Robust Flutter Margins', *J. Aircr.*, vol. 37, no. 6, pp. 1105–1112, 2000.

[6] H. Torii and Y. Matsuzaki, 'Flutter Margin Evaluation for Discrete-Time Systems', *J. Aircr.*, vol. 38, no. 1, pp. 42–47, 2001.

[7] F. Roizner and M. Karpel, 'Linear and Nonlinear Flutter Analyses Using Dynamic Response Computations', in *58th AIAA/ASCE/AHS/ASC Structures, Structural Dynamics, and Materials Conference*, American Institute of Aeronautics and Astronautics.

[8] M. Karpel and F. Roizner, 'Towards Flutter-Boundary Tests with Controlled Vibration Levels', presented at the IACAS 2017 Conference, Tel Aviv, Israel, 2017.

[9] T. Theodorsen, 'General Theory of Aerodynamic Instability and the Mechanism of Flutter', NACA, 496, 1935.

[10] H. J. Hassig, 'An approximate true damping solution of the flutter equation by determinant iteration.', *J. Aircr.*, vol. 8, no. 11, pp. 885–889, 1971.

[11] P. C. Chen, 'Damping Perturbation Method for Flutter Solution: The g-Method', *AIAA J.*, vol. 38, no. 9, pp. 1519–1524, Sep. 2000.

[12] B. Gjerek, R. Drazumeric, and F. Kosel, 'A Novel Experimental Setup for Multiparameter Aeroelastic Wind Tunnel Tests', *Exp. Tech.*, vol. 38, no. 6, pp. 30–43, Nov. 2014.

COPYRIGHT STATEMENT